Yuanyuan Zhou · Zhenming Shi · Tong Qiu · Hongchao Zheng

Original Paper

Failure characteristics of landslide dams considering dam formation features in laboratory experiments

Abstract The geometries and material properties of a landslide dam depend on the dam formation process and affect the breaching process. A comprehensive understanding of the entire process of dam formation and breach is necessary for a more accurate analysis of the dam stability and failure characteristics, but little research has been done in this area. In this study, the effects of debris composition, sliding width, and valley shape on dam breaching by considering dam formation features were experimentally investigated. Results reveal that the stability and failure modes of landslide dams are predominantly governed by the debris composition. The dam stability increases with mean grain size, especially the grain size at the overflow location. Dam height and width are largely influenced by debris composition and sliding width, and the lake volume is highly dependent on the valley shape. The arrival time of peak discharge for balance-grained dams is more related to the dam height than the lake volume, while fine-grained dams are the opposite. The peak discharge is significantly influenced by the lake volume and released water volume, while the effects of dam height, downstream slope, and lake shape coefficient are negligible. Balance-grained dams exhibit two longitudinal evolution models in different shaped valleys. The evolution model of fine-grained dams is different from that of balance-grained dams and is independent of valley shape. This study improves our current understanding of the whole process of landslide dams from formation to failure and the effects of dam formation features on dam breaching.

Keywords Breach evolution · Landslide dam · Overtopping failure · Particle distribution · Valley shape

Introduction

Landslide dams are common phenomena in mountainous regions when the river channels are blocked by avalanches, slides, flows, and glacial ice (Costa and Schuster 1988; Casagli et al. 2003). Due to the complexity and irregularity in their instantaneous formation process, these dams typically comprise of heterogeneous mass of unconsolidated soil and rock materials in an unstable state, making them vulnerable to sudden burst and hence hazardous (Xu et al. 2009; Chang and Zhang 2010; Zhong et al. 2018). Once a landslide dam fails, the outburst floods caused by a rapid release of impound water can exacerbate the scope and scale of the hazard both in space and time (Yin et al. 2009; Fan et al. 2020; Zheng et al. 2022). For example, the largest dam formed during the Diexi earthquake in 1933 broke after 45 days of its formation, resulting in a flood that caused 2500 deaths and affected areas over 250 km downstream (Dai et al. 2021). A catastrophic flood resulting from the failure of

the Yigong landslide dam in 2000 destroyed much of highways, bridges, communication cables, and dense forests across the Yigong River (Shang et al. 2003); the outburst flood traveled over 500 km south into India, with a recorded 5.5-m rise in water level at a distance of 462 km from the breached dam (Delaney and Evans 2015). Therefore, it is a critical issue in risk management and hazard mitigation to evaluate the stability and breaching process of a landslide dam after its formation.

The stability and failure of a landslide dam is affected by many factors that characterize the dam, valley, and hydraulic conditions. The characteristics of the landslide dam (i.e., composition materials, geometry, and particle size distribution) are closely related to the potential energy of the impound water and dam erodibility, influencing the stability of landslide dam and the dam-breach flood (Costa and Schuster 1988; Cui et al. 2009; Fan et al. 2020). Due to the difficulty of field tests, flume tests are commonly used to investigate landslide dam failure by constructing model dams. In these studies, the pre-built dams have regular shapes (i.e., trapezoid or triangle) and homogeneous internal structure. Based on flume model tests, the influence of dam geometry, dam material, and inflow rate on the failure process (Chen et al. 2015; Jiang et al. 2018; Zhu et al. 2020), erosion characteristics, and breach evolution process of landslide dams (Zhou et al. 2019a; Ruan et al. 2021; Zhu et al. 2021) has been studied. Although these studies have built a strong foundation for understanding the instability and breaching process of landslide dams, irregularities in dam deposit morphology and internal structure have not been fully considered. It is unclear whether these research findings are applicable to natural landslide dams. In addition, the valley shape has often been neglected for practical reasons, although it has a profound effect on the geometric characteristics of a landslide dam and lake volume (Walder and O'Connor 1997; Yin et al. 2009).

In fact, the failure of a landslide dam involves a disaster chain consisting of a landslide, dam formation, landslide-dammed lake, and progressive dam failure (Liu and He 2018; Fan et al. 2019, 2020). In existing studies, however, the landslide dam formation and dam failure are treated as two separate processes, ignoring the linkage between them. The dam morphology, a crucial factor for evaluating the hazard of a landslide dam, depends on the formation process relevant to the topography of landslide and valley (Costa and Schuster 1988; Kuo et al. 2011; Zhao et al. 2019; Zhou et al. 2021). The particle size distribution and geotechnical properties at different parts of a landslide dam are quite different due to fragmentation, particle segregation, and different formation processes (Dunning and Armitage 2011; Zhou et al. 2019b, c; Mei et al. 2021). Therefore, it is necessary to investigate the stability and failure of landslide dams considering the process and features of dam formation.
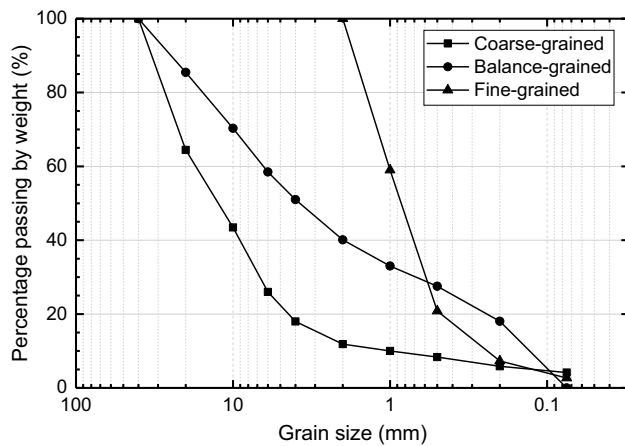
Fig. 1 Grain size distribution of released material

In this study, a series of physical model tests were conducted to reproduce the entire process, involving the deposition of a granular sliding mass into a valley and the formation of a landslide dam. The effects of material composition, width of the sliding path, and valley shape on the stability and breaching process of landslide dams were investigated, providing new insights into the landslide dam failure. In the following sections, the experimental testing program is first presented, followed by descriptions of the dam formation features and failure characteristics of landslide dams. Finally, mechanisms that control the stability and breach process are discussed.

Methods

Experimental materials

The grain compositions of the released material were based on three typical grain size distribution (GSD) curves selected from the Xiaogangjian landslide dam, Donghekou landslide dam, and Tangjiashan landslide dam materials reported by Chang and Zhang (2010) and Chang et al. (2011). Figure 1 shows these GSD curves, which were prepared by mixing silica sand and gravel with different particle sizes. According to the dam material classification proposed by Casagli et al. (2003) and Zhu et al. (2020), the debris types can be regarded as coarse-grained, balance-grained, and fine-grained, which can be classified as GW (well-graded gravel with sand), SP (poorly graded sand with gravel), and SP (poorly graded sand), respectively, according to the unified soil classification system. The coarse-grained debris and balance-grained debris have a

maximum particle diameter of 40 mm, whereas the fine-grained debris has a maximum particle diameter of 2 mm.

Table 1 shows several properties of the released materials. The cohesion of these materials was zero, and the internal friction angles were measured by the draw down test with an upper box (500 mm × 400 mm × 500 mm) and lower box (600 mm × 400 mm × 400 mm) based on Roessler et al. (2019). Considering that the dam deposits were formed by natural accumulation, the densities of the dam deposit were different. Thus, the saturated hydraulic conductivity k of the debris material was measured at the same dry density as the corresponding dam deposits using the constant-head hydraulic conductivity test (Iverson et al. 2010).

Experimental setup

The experimental setup consists of two chutes connected to a horizontal flume of 5.0 m long and 0.4 m wide (Fig. 2a). The two chutes represent the landslide source area and the sliding area, while the flume represents the river valley (Fig. 2a and b). The center line of the chutes was located 3.0 m away from the water intake with an angle of 90°. The upper and lower chutes had respective lengths of 1.5 m and 2.0 m, and the width of sliding path (W_l) could be adjustable. The inclination angles of the upper (β) and lower (α) chutes could be independently adjusted from 20 to 70°. According to the slope data of 84 landslide cases compiled by Fan and Qiao (2010), the angles of the landslide source area and the sliding area were in the range of 26 ~ 59° and 0 ~ 40°, respectively. In this study, the upper and lower chutes were fixed at angles of 45° and 30°, respectively, within the respective ranges. A wood box with dimensions of 0.5 m × 0.4 m × 0.4 m was located at the free end of the upper chute, where the debris material was released via a gate. Three shapes of transverse flume profiles (i.e., rectangular, trapezoidal, and triangular) were used to simulate various transverse characteristics of river valleys, and the cross-sectional area of each flume was constant at 0.12 m² (Fig. 2c). The inflow rate was kept at 1 L/s controlled by an electromagnetic flowmeter and a flow pipe valve.

The lateral walls of the chutes and flume were made of Plexiglass to allow observation. As shown in Fig. 2a and b, four digital video cameras were positioned to record the entire process from the release, to the formation of the dam, and to the potential breaching failure under the constant inflow rate. Cameras 1 and 2 were placed on the two sides of the flume to observe the development of phreatic line and the dam breaching process longitudinally, camera 3 was placed above the dam to observe the overall breaching process, and camera 4 was placed at the end of the flume to observe

Table 1 Properties of test materials

Materials	d_{50}(mm)	C_c	C_u	c (Pa)	φ (°)	ρ_d(g/cm³)	k (10⁻⁴ m/s)
Coarse-grained	12.50	2.7	18.2	0	37.2	1.98	241.1
Balance-grained	3.78	0.6	49.0	0	33	2.02	16.2
Fine-grained	0.86	1.4	4.3	0	27.3	1.70	7.3

d_{50} is the median grain size, C_c and C_u are the coefficient of curvature and coefficient of uniformity, respectively, c and φ are the cohesion and internal friction angle, respectively, ρ_d is the dry density, and k is the saturated hydraulic conductivity
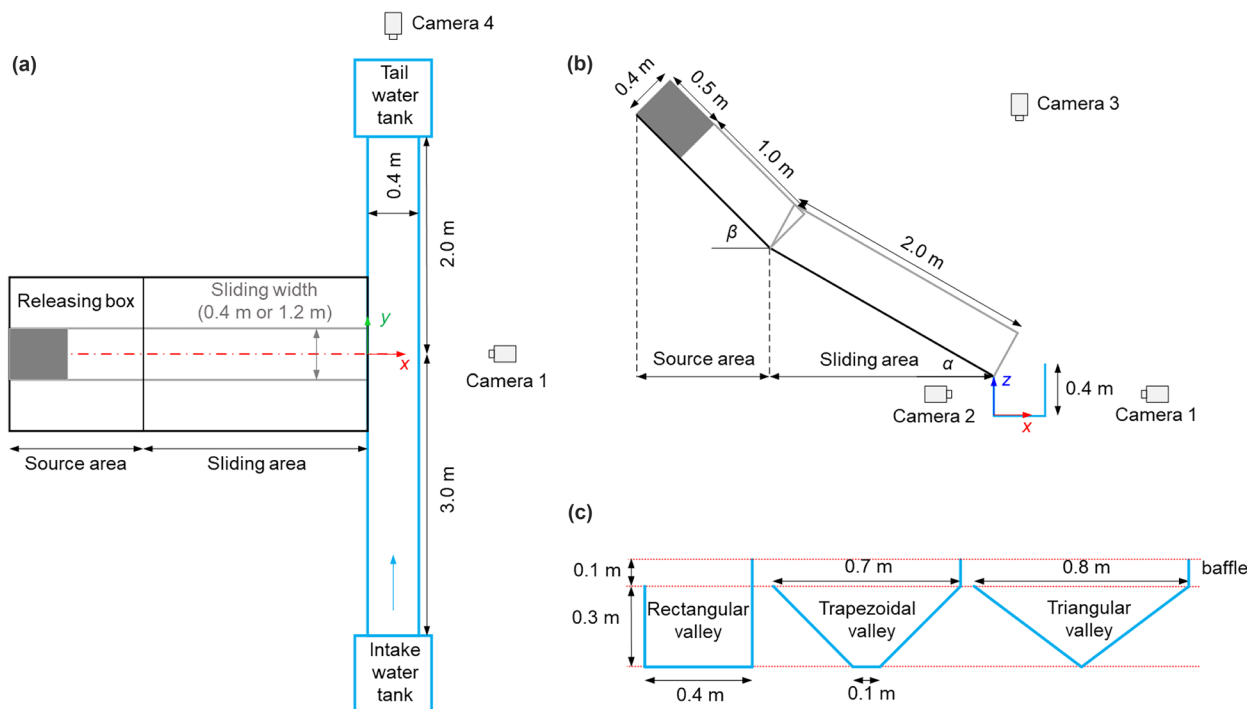
Fig. 2 Experimental setup: (**a**) top view; (**b**) side view; (**c**) geometry of three flume profiles

the progression of the breach width and depth. A 3D laser scanner was employed to obtain the morphological parameters of the dam deposit after dam formation and dam failure.

Experimental design and procedure

The purpose of this study is to investigate the effect of dam characteristics under different conditions, including the GSD of sliding materials, sliding width, and valley shape, on landslide dam stability and failure process. Thus, the relevant parameters varied in the experiments were the material composition (i.e., coarse-grained, balance-grained, and fine-grained), width of sliding path (i.e., 0.4 m and 1.2 m), and shape of transverse flume profiles (i.e., rectangular, trapezoidal, and triangular). A total of 18 tests were designed and shown in Table 2. In the test designation, N and W stand for the sliding width of 0.4 m and 1.2 m, respectively; 1, 2, and 3 stand for rectangular, trapezoidal, and triangular valley, respectively; and C, B, and F stand for coarse-grained, balance-grained, and fine-grained,

respectively. For example, Test N-1C corresponds to a test done on a sliding width of 0.4 m (i.e., N) with the rectangular valley (i.e., 1) using coarse-grained debris (i.e., C).

For each test, the experimental setup was first adjusted to the test condition; the dry debris with all grains mixed uniformly was then released onto the upper chute and flowed into the river flume to form a landslide dam. The dam profile was scanned using a 3D laser scanner. Next, water was discharged into the flume at 1 L/s. After the breach profile reached constant or the outflow discharge remained equal to the inflow rate within 15 min, the breach process was considered to have ended. Finally, the residual dam profile was scanned.

Characteristics of dam deposits

Parameter definition

Different from previously tested dams which were pre-built in the flume, in this study, the morphology of dam deposits was irregular, and the particle distribution of dam deposits was heterogeneous.

Table 2 Test matrix

Material	Rectangular valley (1)		Trapezoidal valley (2)		Triangular valley (3)	
	W_i: 0.4 m	1.2 m	0.4 m	1.2 m	0.4 m	1.2 m
C	N-1C	W-1C	N-2C	W-2C	N-3C	W-3C
B	N-1B	W-1B	N-2B	W-2B	N-3B	W-3B
F	N-1F	W-1F	N-2F	W-2F	N-3F	W-3F

After processing the point clouds from the 3D laser scanner, the geometric parameters such as dam width (W_d), dam height (H_d), downstream slope (θ_d), crest surface frontal angle (θ_c), and lake volume (V_l) were obtained (Fig. 3). Dam width was characterized as the maximum width of the landslide dam measured along the river valley, neglecting the splash particles (which were disconnected from the main deposit); dam height was the height from the overflow point to the riverbed; crest surface frontal angle was the angle between the tangential line of the dam profile from the overflow point and the horizontal plane; and lake volume was the volume of dammed lake when the water level reached the overflow point. The downstream slope was measured on the longitudinal section through the overflow point in the case of rectangular valley and the longitudinal section across the centerline of the river valley in the cases of trapezoidal and triangular valley.

Geometrical parameters

Figure 4 shows the relationships between the geometry of dam deposits and the sliding path width, GSD of the material, and valley shape. The dams had lower height but higher width for W_l= 1.2 m than those for W_l= 0.4 m because the sliding mass can spread laterally along the chute with W_l= 1.2 m before entering the valley, producing a relatively wider and lower deposit. As the gravel content decreased from coarse-grained to balance-grained to fine-grained, the dam height decreased almost linearly, except for the tests in rectangular valley with W_l= 1.2 m (Fig. 4a). As the mean grain diameter decreased, the flow-front velocity into the valley decreased from 4.75 to 3.64 m/s. The number of particles reaching the opposite side also decreased, lowering the dam height. However, for the tests in rectangular valley with W_l= 1.2 m, the dam height shows an opposite trend, because the deposit was higher on the opposite side and the dam height was measured on the source side of coarse-grained and balance-grained dams.

The downstream slope of the dam deposits varied from 14 to 29° (Fig. 4c). This is consistent with the range of slope angles of 11 ~ 45° for natural landslide dams (Zheng et al. 2021). The angle of downstream slope was larger for W_l= 0.4 m than that for W_l= 1.2 m due to the confinement of the sidewall during sliding. The fine-grained dams generally have the smallest downstream slope angle among the three debris compositions tested due to its small internal friction angle (see Table 1). Test W-1C was an exception because the dam height was too small on the source side.
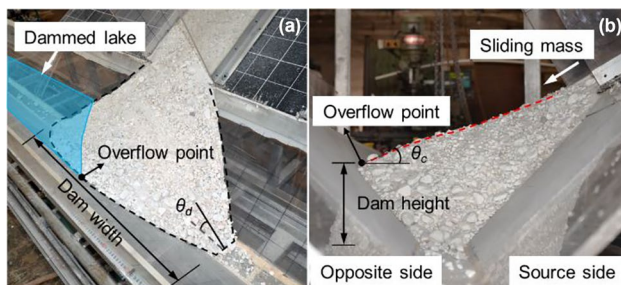
The crest surface frontal angle can be used as a parameter to infer the stability of the dam in cross-valley direction. A higher crest surface frontal angle implies that the dam crest is more prone to slump when breach erosion occurs. Figure 4d shows that the crest surface frontal angle increases with the decrease of mean grain diameter. Comparing θ_c values between the two sliding widths suggests that the width of sliding path has little effect on the crest surface frontal angle. Test W-1C and Test W-1B as exceptions have a negative value which indicates that the overflow point is located on the source side.

In addition to dam geometry, the volume of dammed lake which is related to the potential energy of impound water is an important parameter affecting dam failure (Costa and Schuster 1988). The volume of dammed lake is mainly determined by the dam height and valley shape. The variation of the dammed lake volume with valley shape is shown in Fig. 5. Evidently, the volume of dammed lake was larger for W_l= 0.4 m than that for W_l= 1.2 m due to the higher dam height. In general, the volume of dammed lake decreased as the valley shape changed from rectangular to trapezoidal to triangular, except when the dam height in the rectangular valley was very small, such as the tests in rectangular valley with W_l= 1.2 m (i.e., Tests W-1C and W-1B).

Particle distribution

The selected PSDs have amplified particle segregation in this study. All the debris grains were homogenously mixed prior to release. Grain segregation occurred during the flow and deposition process. On the surface of the final dam deposit, fine sand particles were concentrated on the source side (Fig. 6b), and the coarse gravel particles were mainly concentrated at the distal end and near the opposite side (Fig. 6c). Furthermore, the coarse particles were more distributed in the surface layer of the deposit and less in the interior (Fig. 6d and e). This phenomenon is in accordance with the experimental observations of Schilirò et al. (2019) that rock avalanche deposits have an upper carapace facies mainly composed of coarse grains and a lower portion relatively rich in fine particles.

Scaling validation

Scaling plays a crucial role in physical modeling experiments and can be addressed by using dimensional analysis (Iverson 2015). Unlike most prebuild dams, the landslide dams in this study were formed through a deposition process mimicking natural conditions; thus, there is no particular scale and regular dam shape. Peng and Zhang (2012) proposed three dimensionless coefficients ($\frac{H_d}{W_d}$, $\frac{V_d^{1/3}}{H_d}$, and $\frac{V_l^{1/3}}{H_d}$), based on 1239 landslide dam cases, to determine the geometrical characteristics of landslide dams and dammed lakes, affecting the breaching process. Zhou et al. (2019a) verified the reasonableness of a modeled dam by comparing these dimensionless coefficients with those of landslide dams in the field. The three dimensionless coefficients of the dams in this study were evaluated against those of 250 landslide dams derived from the worldwide landslide database (Shen et al. 2020). Figure 7 shows the relationship between the ratio of dam height to dam width ($\frac{H_d}{W_d}$),


Fig. 3 Geometric parameters of dam deposit: (**a**) isometric view; (**b**) side view (from downstream)

Fig. 4 Variation of dam geometries with debris composition: (**a**) dam height; (**b**) dam width; (**c**)downstream slope; (**d**) crest surface frontal angle
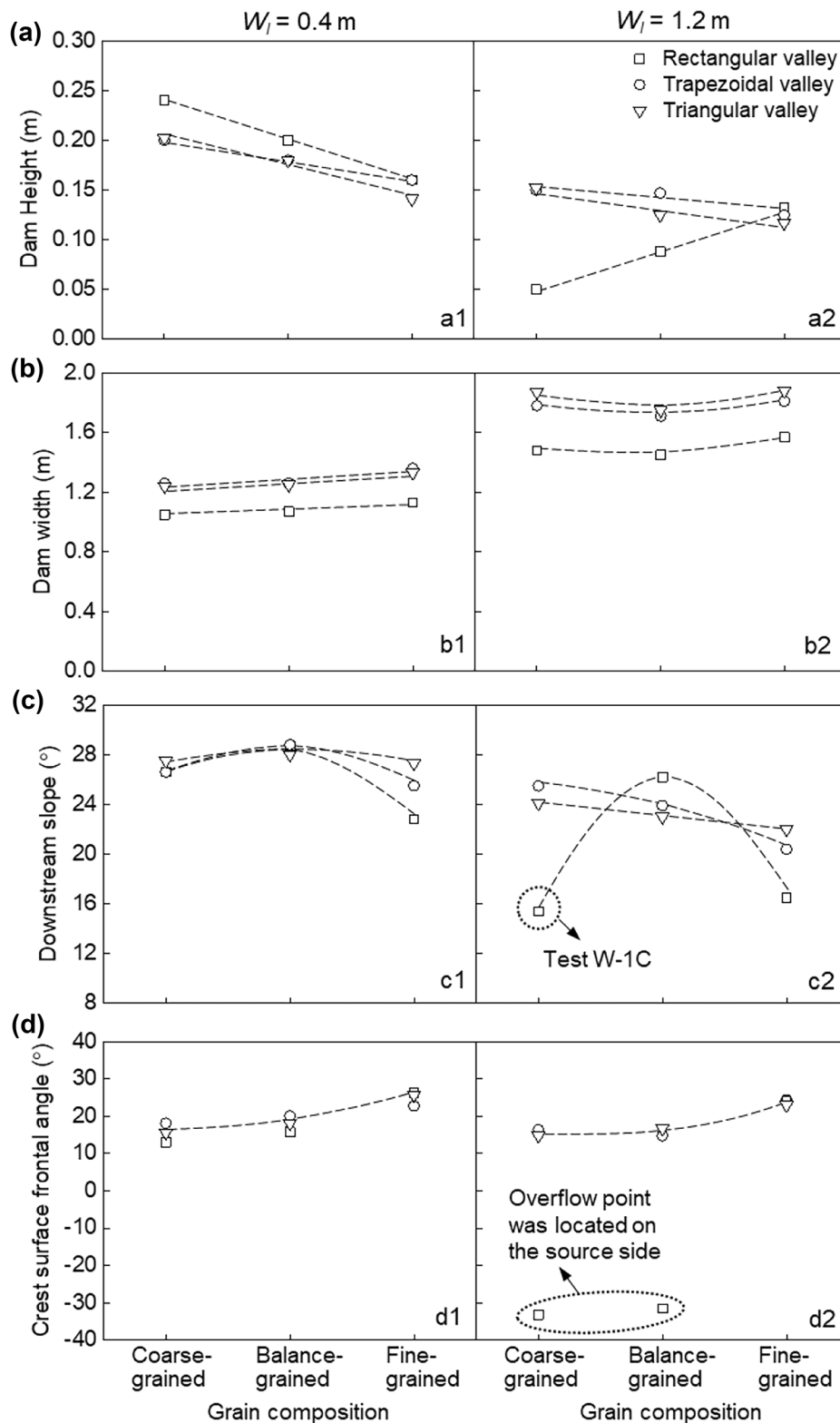
dam shape coefficient ($\frac{V_d^{1/3}}{H_d}$), and lake shape coefficient ($\frac{V_l^{1/3}}{H_d}$). The dimensionless coefficients of all tested dams in this study were within the range of field data, suggesting that the dam deposits and dammed lake in the experiments have realistic geometrical characteristics and can be considered to represent natural landslide dams and dammed lakes.

Fig. 5 Variation of dammed lake volume with valley shape: (**a**) $W_l = 0.4$ m; (**b**) $W_l = 1.2$ m
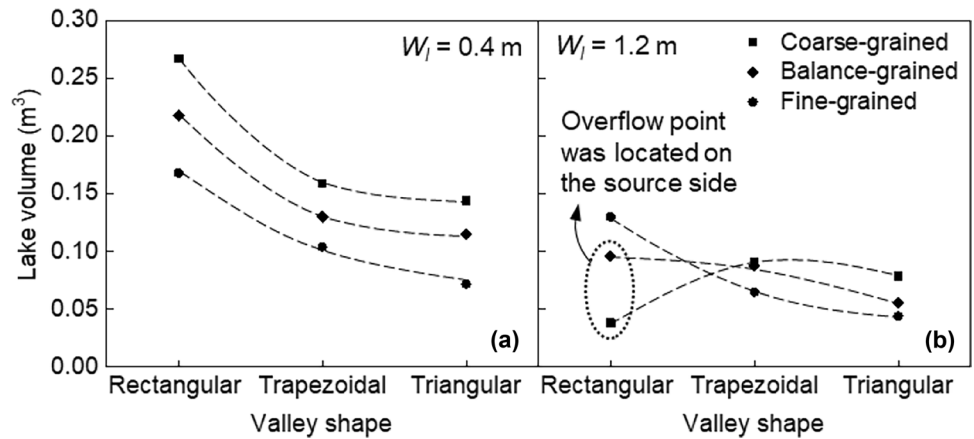
Failure characteristics of dam deposits

Failure types of dam deposits
Seepage equilibrium under overtopping

Figure 8 shows typical features of a stable dam formed by coarse-grained debris using Test N-3C as an example. At $T = 0$ s, water started to enter the flume from the intake tank (Fig. 2). As water level rose gradually, a seepage path formed inside the dam. The seepage flow appeared at the toe of the downstream slope at $T = 111$ s (Fig. 8a) due to a relatively high hydraulic conductivity (Table 1); as the water level continued to rise, water overflowed the dam crest at $T = 286$ s (Fig. 8b). Eventually, the inflow discharge was balanced by the seepage flow and the overflow, with the upstream water level at 0.23 m. The dam deposits remained stable, which corresponds to the case of overtopping without erosion in the classification of Xu et al. (2009).

The coarse-grained debris is classified as a well-graded gravel with sand, in which coarse gravel particles are the dominant constituents. Although a complete seepage path formed easily in the dam deposits and few fine sand particles were eroded by the seepage flow, the internal structure remained stable. Moreover, due to

Fig. 6 Particle distribution of dam deposits: (**a**) isometric view (from upstream); (**b**) portion of the rear of dam deposits (A zone); (**c**) portion of the distal of dam deposits (B zone); (**d**) residual dam after breaching; (**e**) portion of interior of dam deposits (C zone)

segregation, the debris at the overflow point was mostly coarse gravel particles which are not vulnerable to erosion; hence, the surface of the dam was not eroded by overflow.

Overtopping with scarp erosion

As shown in Fig. 9, the geometry of the dam formed was not as regular as a trapezoid. For simplicity, points A and B are considered the turning points on the dam crest for subsequent analysis. Point A is where the water flow velocity begins to increase, and point B is the intersection between the horizontal line passing point A and the upstream slope.

For balance-grained dams, there was no complete seepage path through the dam body when overflow occurred due to a relatively low hydraulic conductivity (Table 1). When water reached point A, we set $t = 0$ s as the beginning of overtopping. The erosion scarp was first to form as some of the fine sand particles from a part of the downstream face were eroded away by the flowing water exceeding the critical shear stress (Fig. 9a). As such, some of gravel particles stayed in place, while coarse sand particles were moved and deposited nearby (Fig. 9b). As an increasing number of sand particles were eroded away, coarse gravel particles rolled over due to the loss of support from surrounding sand particles. A channelized flow was formed, and the scarp progressed towards the dam crest (Fig. 9c). When the erosion reached point B, an outburst flood started to develop, further entraining the debris, and the erosion process progressed further upstream with the toe of the dam eroded (Fig. 9d). From then on, the water level decreased rapidly as the upstream slope was eroded, accelerating the erosion process. Meanwhile, lateral erosion continued to develop and side slope of the breach channel close to the downstream collapsed into the breach channel (Fig. 9e). Subsequently, new erosion scarps were formed on the longitudinal profile, and continual erosion and collapses occurred on the side slope of breach channel (Fig. 9f). The fine particles of the blocks slumped from the channel bank were eroded away, while the coarse ones lodged in the channel and were progressively eroded (Fig. 9g). The breach bottom began to flatten out from a wavy shape as the erosion subsided. Eventually, the water level decreased to a constant, the water flow velocity decreased to a value that could no longer erode the residual material, and the coarse particles on the bottom of the breach formed an armoring layer, preventing further vertical erosion (Fig. 9h).
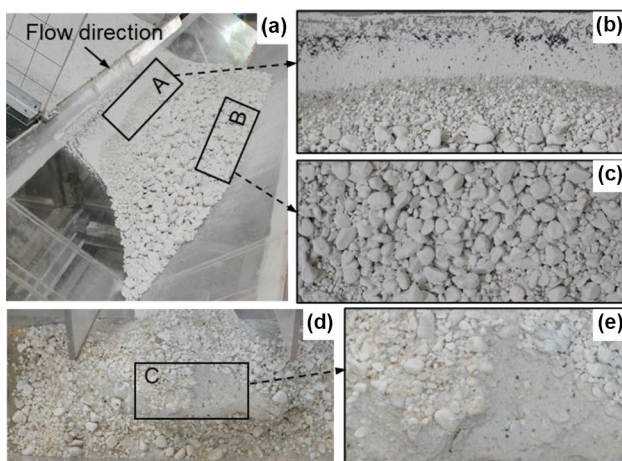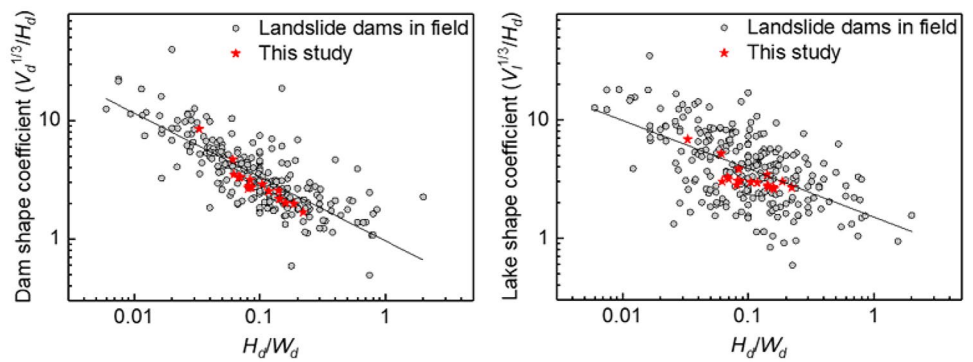
Overtopping with layered erosion

The fine-grained dams all failed due to overtopping with layered erosion. Similar to the observations of balance-grained dams, seepage flow was not observed at downstream when overflow occurred. Using Test N-1F as an example, Fig. 10 shows that water flow gradually eroded sand particles layer by layer, forming a smooth surface that progressed downwards and upstream. Because the fine-grained debris without gravel had a lower shear strength, erosion began as soon as water overtopped the dam crest, even the initial overtopping flow was shallow (approximately 4 mm), and the flow velocity was small (approximately 0.1 m/s) (Fig. 10a). With time, the eroded area expanded rapidly and advanced upstream. At $t = 29$ s, a round-shaped dam crest formed, and the erosion advanced rapidly and was accompanied by multiple collapses or slides of the breach channel slope (Fig. 10b–d). With time, the flow gradually slowed down, and the breach bottom began to flatten out (Fig. 10e and f). Eventually, the geometry of the breach reached constant, leaving an almost asymptotically stable "equilibrium" dam surface. The breaching process of the fine-grained dams can be characterized as more orderly due to the finer nature of the gradation, without steep erosion scarp during the entire erosion process. Similar processes

Fig. 8 Stable dam formed by coarse-grained debris: (**a**) seepage occurrence; (**b**) overflow occurrence (view from Camera 3)
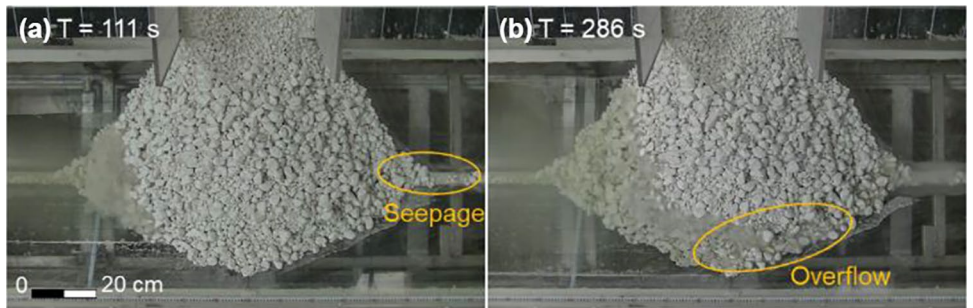

Fig. 9 Breaching process of balance-grained dam in Test N-1B
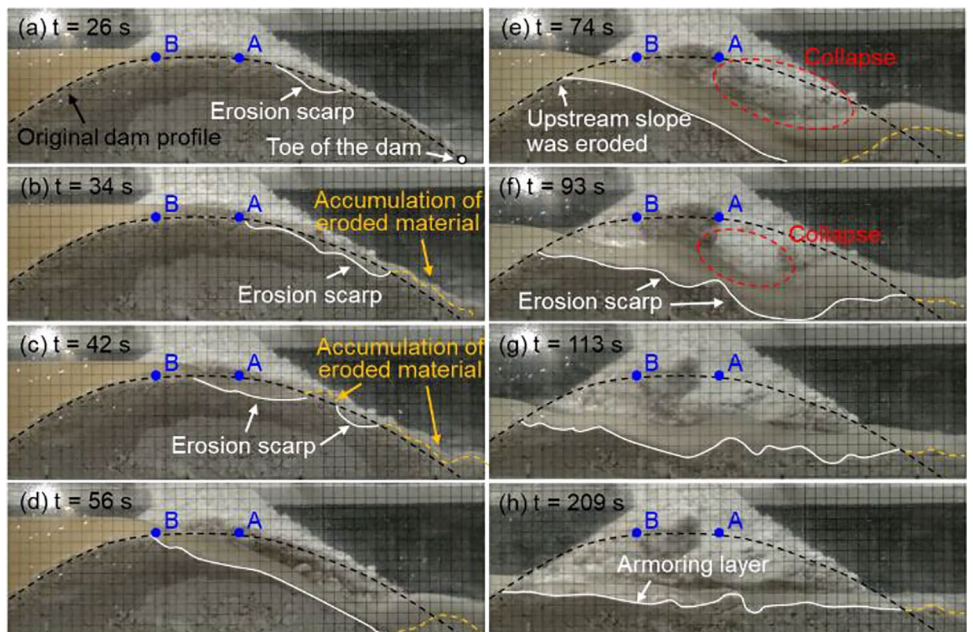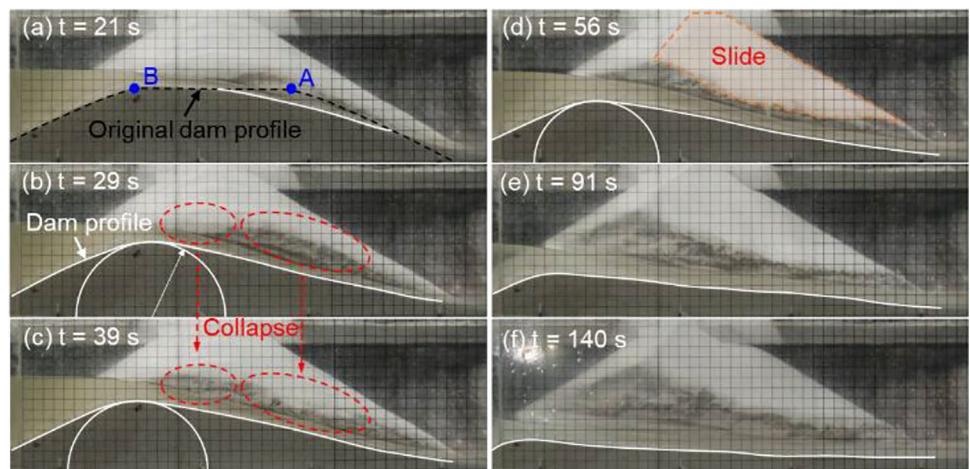
Fig. 10 Breaching process of fine-grained dam in Test N-1F

were observed by Chinnarasri et al. (2003) and Schmocker and Hager (2009) in experiments with similar GSD of sands.

Partial failure without decrease in dam height

The dam deposits in Tests W-3B and W-1C suffered local instability, but the dam height did not decrease at the inflow rate of 1 L/s. The overtopping water over the dam crest just eroded a channel along the downstream face of the dam. The breach channel did not reach the upstream of the dam after a steady state was reached, and the total height of the dam was not reduced. Figure 11 shows the comparisons of dam morphology before breaching and after breaching in these tests. It can be observed that just a small amount of sand particles on the downstream face and toe of the dam were eroded away in Test W-3B (Fig. 11(a2)). Based on the hydraulic flow regime proposed by Powledge et al. (1989), the hydraulic force and energy level were low on the dam crest, and increased at the downstream edge of the crest, where the erosion can occur. However, due to the wide sliding path, the dam deposit had a larger width and lower height with $\frac{H_d}{W_d} = 0.07$ (Fig. 4a and b). Moreover, the upstream reservoir was the smallest (i.e., 0.056 m³) among all tests of balance-grained dams because of the dam height and triangular valley (Fig. 5). Consequently, the hydraulic forces were not large enough to erode the large particles or enlarge the surface discontinuities to destabilize large particles.

Test W-1C was an exception for coarse-grained dams where the dam deposit was higher on the opposite side, and the overflow point was on the source side where the fine particles were concentrated on the surface, resulting in a less stable structure more vulnerable to erosion, as shown in Fig. 11(b1) and (b2). Due to the low dam height (i.e., 0.05 m) and limited lake volume (i.e., 0.038 m³), the erosion process only occurred on the downstream slope near the source side and dam crest near the downstream slope. The dam erosion ceased before the breach channel was completely developed, and the eroded material was redeposited downstream near the dam (Fig. 11(b2)).

Breaching stages and breaching discharge

According to the definition of longevity of landslide dams (Shen et al. 2020) and the hydrological evolution process, the failure process of a landslide dam in this study was divided into four stages: (i) water infilling, (ii) dam overflowing, (iii) dam breaching, and (iv) river rebalancing. As shown in Fig. 12a, stage (i) started when the upstream flume began to fill water ($T = 0$ s) and ended when the overflow began (point A). Stage (ii) referred to the formation of the initial breach, when the downstream surface of the dam began to erode, causing a small increase in the outflow discharge. During stage (ii), the upstream water level continued to rise until reaching its maximum. Stage (iii) referred to the period from the

Fig. 11 Partial failure of landslide dam: (**a1**) Test W-3B, before breaching; (**a2**) Test W-3B, after breaching; (**b1**) Test W-1C, before breaching; (**b2**) Test W-1C, after breaching
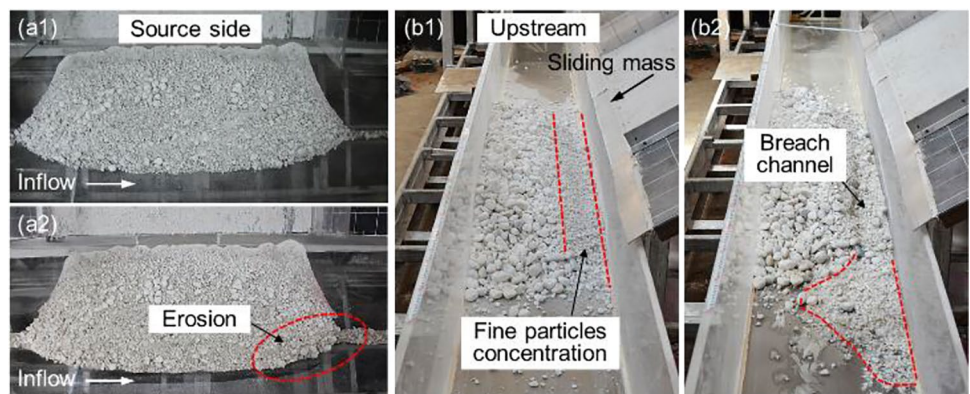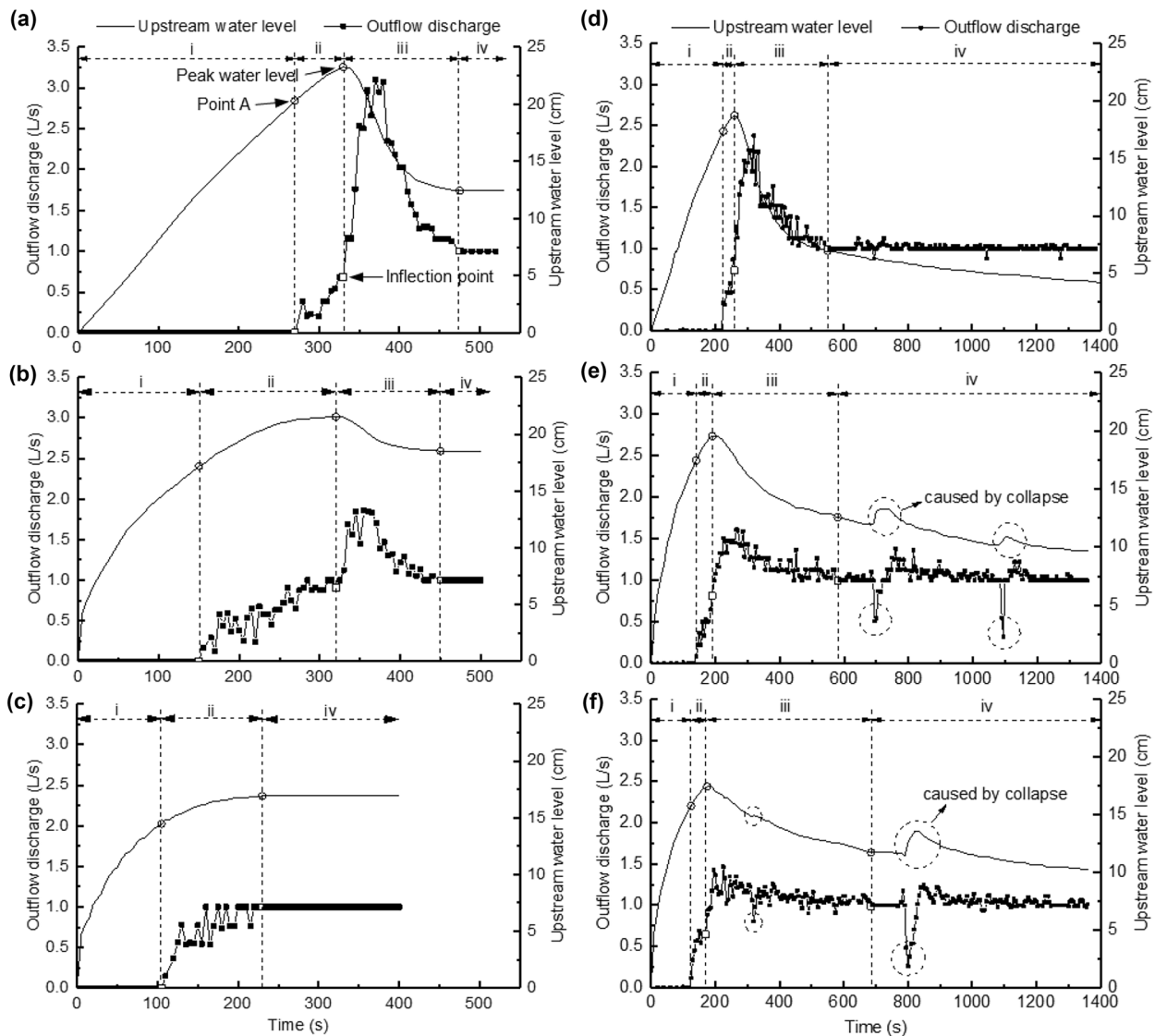
Fig. 12 Variation in upstream water level and outflow discharge of landslide dams: (**a**) Test N-1B; (**b**) Test N-3B; (**c**) Test W-3B; (**d**) Test N-1F; (**e**) Test N-2F; (**f**) Test N-3F

erosion of the upstream slope to the end of dam breaching, which was the main stage of the breach growth. As the sudden decrease of the elevation of the breach entrance due to collapse, the outflow discharge increased suddenly (e.g., inflection point in Fig. 12a) and then decreased after reaching a maximum value. Stage (iv) was the period of river re-equilibrium, when the outflow discharge asymptotically balanced with inflow and the reservoir water level became stable.

The upstream water level and the outflow discharge continuously evolved during the breaching process (Fig. 12). Balance-grained dams had a shorter longevity (less than 600 s) than fine-grained dams (about 1400 s) due to the formation of the armoring layer that prevents further erosion in the former. For balance-grained dams, the discharge hydrographs were classified into three types base on their variation characteristics (Fig. 12a–c). The first type, as shown in Fig. 12a, was a typical breach discharge

hydrograph of a landslide dam, which was consistent with the experimental results of many investigations in a rectangular flume (Yang et al. 2015; Jiang et al. 2018). The discharge curve from the initial erosion to breach completion can be described as "sharp rise and drop," where the duration of stage (ii) is less than that of stage (iii). The discharge curves of balance-grained dams in rectangular valleys are of this type. In contrast, the second type was described as "slow rise and rapid drop," with the duration of stage (ii) being greater than that of stage (iii) (Fig. 12b). This indicates that the initial breach was formed slowly, leading to a slow growth in outflow discharge. The discharge curves of balance-grained dams in trapezoidal and triangular valleys mostly belong to the second type. The last type was described as "slow rise and no drop," without stage (iii) in the breaching process (Fig. 12c). The outflow discharge increased gradually until reaching the inflow rate, with no drop in the upstream water level. This corresponds to the partial failure of

the dam, where the initial breach did not progress to the upstream slope as shown in Fig. 11.

The hydrographs of fine-grained dams had a similar shape and variation trend, as shown in Fig. 12d–f. Compared to balance-grained dams, the discharge hydrographs belong to the first type. In stage (iv), due to the finer nature of the fine-grained debris, the outflow discharge fluctuated around 1 L/s with a range of ± 0.1 L/s, and the flow was still very slowly eroding the fine particles at the bottom of the breach. As the erosion continued slowly, the lateral slope of the breach channel became more vulnerable to collapse due to the low strength and large crest surface frontal angle (Fig. 4d). The collapsed block may block the breach channel, especially in the trapezoidal and triangular valleys, causing the upstream water level to rise and the outflow discharge to decrease (Fig. 12e and f). However, after a brief decrease, the discharge increased immediately, slightly exceeding the inflow but less than the peak.

The duration of each stage of breaching process and the arrival time of peak discharge (red lines) are shown in Fig. 13. The first two stages, stage (i) and stage (ii), accounted for a larger proportion (over 60%) of the breaching process for balance-grained dams but a smaller proportion (about 30%) for fine-grained dams. This was because the formation of the initial breach of a balance-grained dam took longer (i.e., stage (ii)) due to a higher shear strength of the debris and the progression of erosion scarps. By contrast, during the breach development stage (i.e., stage (iii)), the armoring layer formed quickly due to the large uniformity coefficient of the debris material, and the breach stabilized quickly with the release of water. It took less than 100 s from the arrival of peak discharge to the end of dam breaching. However, a breach in a fine-grained dam was easily formed (less than 90 s) by overflowing water that directly entrained the fine particles at the dam crest; on the other hand, the river took longer to regain equilibrium due to the low strength of fine-grained debris and prolonged erosion process.

In general, the peak discharge occurred earlier for W_l = 1.2 m than that for W_l = 0.4 m (Fig. 13). For fine-grained dams, the arrival time of peak discharge became earlier as the valley shape changed from rectangular to trapezoidal to triangular. For balance-grained dams, however, the variation of peak arrival time with valley shape was not obvious. By comparing the dam height and lake volume in different shape valleys (Figs. 4a and 5), it can be found that

the arrival time of peak discharge was delayed with the increase in dam height H_d and lake volume V_l (Fig. 14). With a higher R^2 value, the arrival time of peak flow is more related to H_d than V_l for balance-grained dams, while the opposite correlation is true for fine-grained dams. This is because the initial erosion of fine-grained dams occurs once the overflow occurs, and the erosion process depends on lake volume; however, the surface erosion of balance-grained dams is affected not only by lake volume but also by particle distribution.

The peak discharge (Q_p) of a landslide dam is usually considered to be closely related to the dam height, lake volume, or a combination of both. Some scholars have proposed empirical models for predicting peak discharge based on landslide dam failure case histories (Table 3). The peak discharge of dams tested in this study is more related to dammed lake volume (V_l) and volume released (V_0) during flood than dam height (H_d) and lake shape coefficient ($\frac{V_l^{1/3}}{H_d}$) (see Fig. 15). Especially, V_0 has the most significant effect on the peak discharge, with R^2 greater than 0.9. For balance-grained dams, the peak discharge is linearly correlated with V_0, while for fine-grained dams, it is exponential. In addition, the peak discharges of balance-grained dams are larger than those of fine-grained dams with the same V_0 (Fig. 15d). This is attributed to a shorter stage (iii) of balance-grained dams (Fig. 13). Once the erosion of surface particles is initiated, the reservoir water will drain in a short time, leading to a large peak discharge.

Development of breach

Based on the experimental observation, three evolution processes of longitudinal profiles of the dams were observed and simplified into three corresponding models, as shown in Fig. 16. For a balance-grained dam, the initial erosion always began on some weak part of the downstream face and then progressed towards dam crest (Fig. 16(a1) and (a2)). As shown in Fig. 16(a1), the erosion rate of Test N-1B was in such a way that the downstream slope angle remained constant initially, and the erosion rate decreased along the flow direction after the upstream slope was eroded, causing the downstream slope to rotate counterclockwise around a fixed pivot point (r_c). This evolution process is characterized by a combination of two theoretical models: one assumes that the downstream
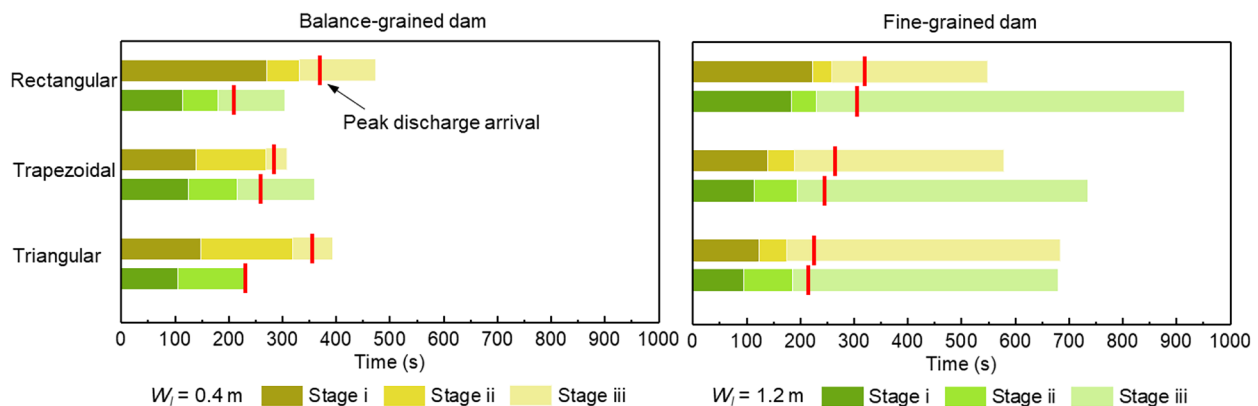

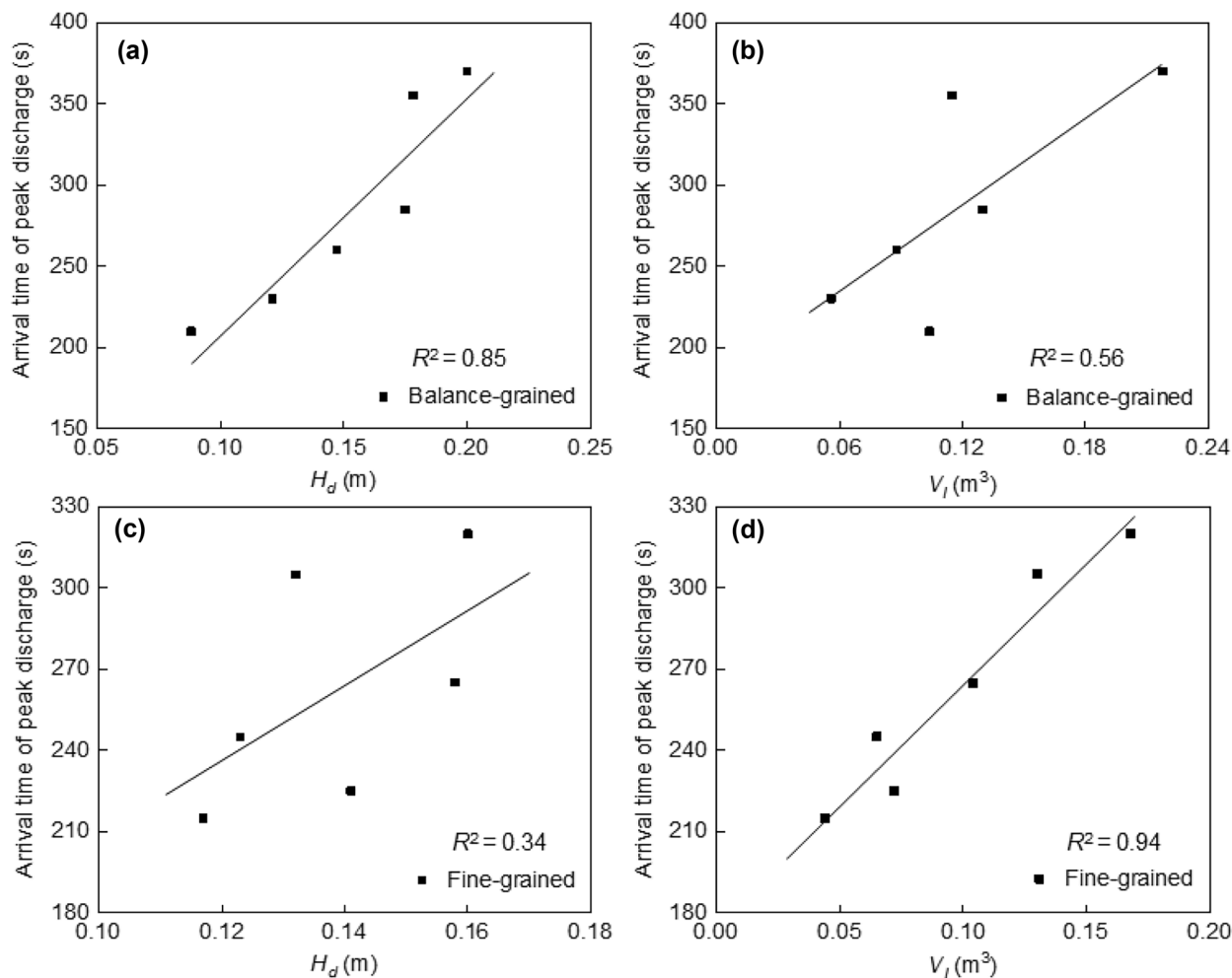**Fig. 13** Stages of breaching process and arrival time of peak discharge

Fig. 14 Relationship between arrival time of peak discharge and dam height and lake volume

slope angle remains constant or increases to a specific value and then remains constant (Visser 1998; Chang and Zhang 2010) and the other considers that the downstream slope angle gradually decreases by rotating along a pivot point at the dam toe with continuing erosion (Zhong et al. 2018), as shown in Fig. 16b. A plausible explanation could be that the growth rate of upstream water level in the rectangular valley is higher than that in the trapezoidal and triangular valleys at the beginning of the breach, resulting

Table 3 Empirical models for peak discharge of landslide dam failure

Equations	References
$Q_p = 6.3H_d^{1.59}$	Costa 1985
$Q_p = 672V_l^{0.56}$	Costa 1985
$Q_p = 1.6V_0^{0.46}$	Walder and O'Connor 1997
$Q_p = g^{0.5}H_d^{2.5}(H_d/H_r)^{-1.371}(V_l^{1/3}/H_d)^{1.536}e^a$	Peng and Zhang 2012

H_d dam height, V_l dammed lake volume, V_o volume released, e^a dam erodibility coefficient, $H_r = 1$ m

in a higher head. Therefore, there is a higher erosion rate of the breached water flow, and the energy of water is sufficient to keep a constant erosion rate at the beginning of the breaching process; as the energy decreases over time, the erosion rate decreases along the flow direction.

The erosion profiles of balance-grained dams in trapezoidal and triangular valleys were concave along the longitudinal flow direction, corresponding to the erosion model proposed by Zhou et al. (2019a) (Fig. 16c) where r_1, r_2, and r_3 represent the trajectory of the erosion point along the downstream slope at different time. However, the trajectory of the erosion point along the downstream slope observed in this study is different than that observed in previous studies. Furthermore, the erosion point does not reach the dam toe throughout erosion because the erosion of most coarse debris cannot progress downstream too far due to insufficient hydrodynamic forces, resulting in the accumulation of coarse particles nearby and forming an armoring layer. On the one hand, due to the bottom widths of triangular and trapezoidal valleys being narrow, the sedimentation of eroded material moves the erosion point up towards the dam crest, and the armoring layer provides hydraulic resistance against further erosion.

Fig. 15 Relationship between peak discharge and geometric parameters of landslide dam: (**a**) Q_p vs H_d; (**b**) Q_p vs V_l; (**c**) Q_p vs $V_l^{1/3}/H_d$; (**d**) Q_p vs V_0
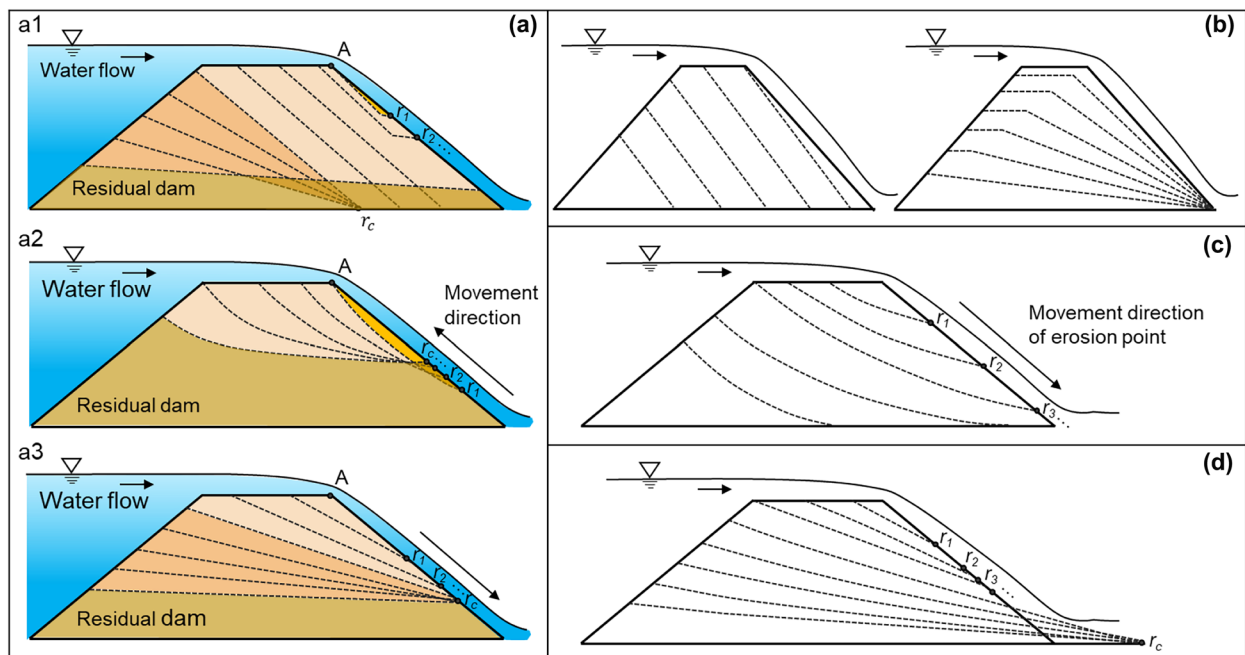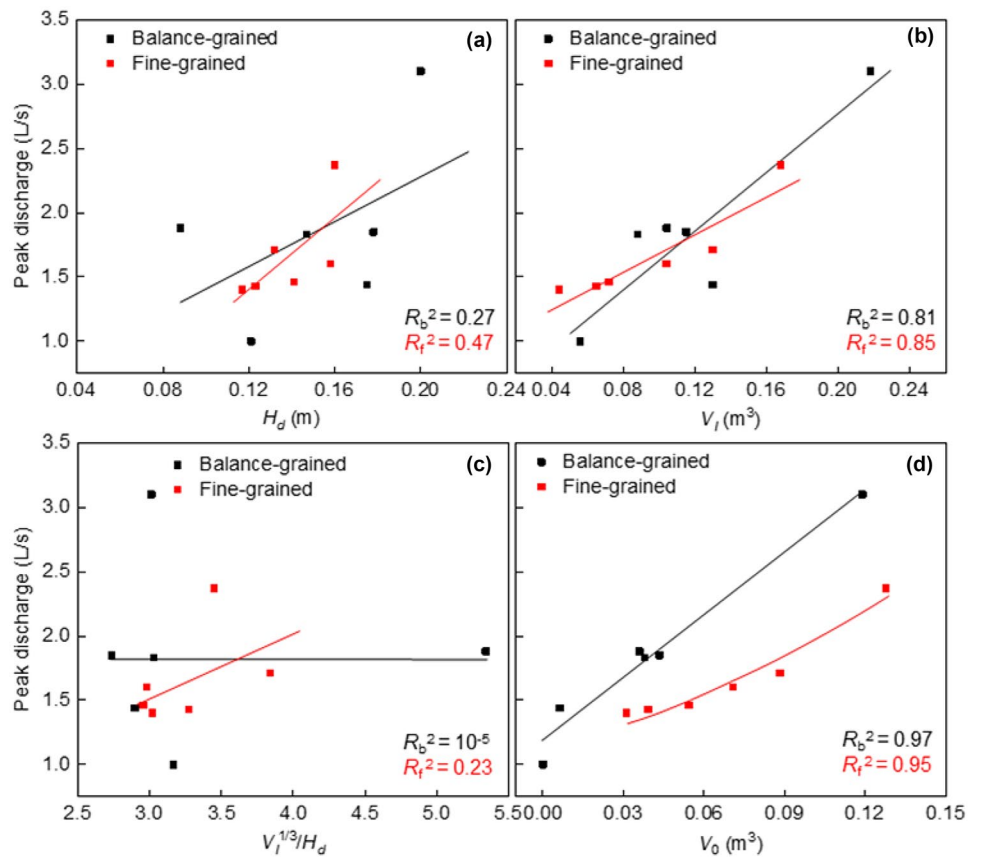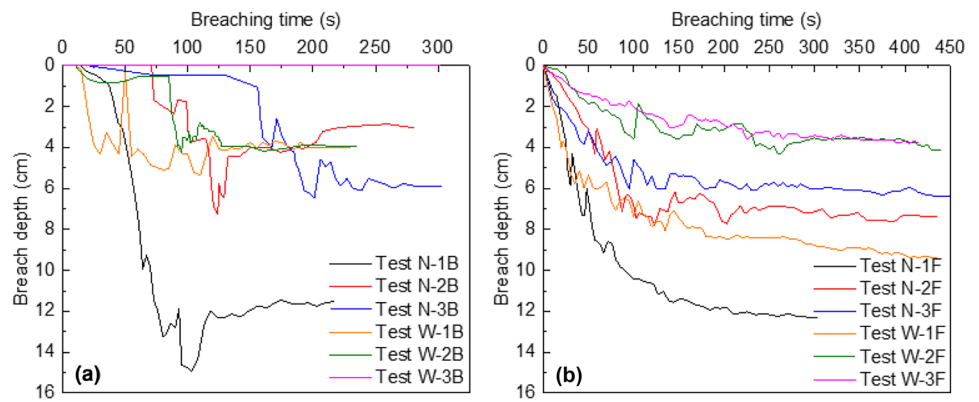

Fig. 16 Longitudinal evolution models of breach profiles: (**a**) this study; (**b**) left proposed by Visser (1998), right proposed by Zhong et al. (2018); (**c**) proposed by Zhou et al. (2019a); (**d**) proposed by Zhang et al. (2021)

Fig. 17 Development of breach depth (water reached Point A at t = 0 s): (**a**) balance-grained dams; (**b**) fine-grained dams

All the fine-grained dams showed similar longitudinal evolution process as shown in Fig. 16(a3), regardless of the valley shape. The erosion began at point A because fine-grained debris had a low shear strength. The erosion point progressed upstream and downstream simultaneously. The erosion rate decreased along the flow direction and the downward direction. This process corresponds well with the evolution model proposed by Zhang et al. (2021), except for the position of the fixed pivot point (r_c) (Fig. 16d). In this study, the erosion point moved along the downstream slope to the dam toe until reaching a fixed pivot point, around which the downstream slope rotated counterclockwise. This indicates that the erosion rate decreases along the flowing direction and becomes almost zero at the downstream slope as erosion progresses. Compared with the scarp erosion of balance-grained dams, the surface erosion of fine-grained dams was uniform throughout the breaching process.

The drop in height at point A of breach bottom was selected as the proxy for breach depth for analysis of breach depth development with time (Fig. 17a and b). Since the erosion occurred at the downstream slope at the beginning of dam overflow, rather than at point A (see Fig. 16(a1) and (a2)), the breach depth of balance-grained dams was almost zero initially (Fig. 17a). As the valley shape changed from rectangular to trapezoidal to triangular, the upstream storage capacity decreased by 37–50%, and the beginning of rapid increase in breach depth was delayed. The breach depth of fine-grained dams, however, increased from $t = 0$ s (Fig. 17b) because the erosion began at point A (Fig. 16(a3)). The change rate of breach depth was regarded as the vertical erosion rate, which changed with time. For a balance-grained dam, the vertical erosion rate is the average rate of change in breach depth during the

rapid change phase, and for a fine-grained dam is the average rate of change in breach depth during the first 50 s. Figure 18 shows that the vertical erosion rates of balance-grained dams and fine-grained dams both increased with dammed lake volume. In addition, the vertical erosion rate rapidly became 0 mm/s after the formation of armoring layer for a balance-grained dam but gradually decreased with time until approaching 0 mm/s eventually for a fine-grained dam (Fig. 17a and b).

Discussion

Effects of debris composition on dam breaching

The GSD of the slide material is a critical factor influencing the landslide dam stability and failure characteristics. Based on the total results of 18 tests in this study, overtopping occurred in all tests. Among them, the coarse-grained dams were stable under overtopping except for Test W-1C; the balance-grained dams failed by scarp erosion, except for Test W-3B with partial failure; and the fine-grained dams all failed by overtopping in the form of layered erosion. As the mean grain size decreases, the dam becomes increasingly unstable with higher chances of overtopping failure, due to a combination of lower shear strength, lower hydraulic conductivity, and higher erodibility associated with the finer gradation (Table 1).

The breach processes of balance-grained dams and fine-grained dams are different, although both involve overtopping. The balance-grained debris has a wide size distribution and a large uniformity coefficient, resulting in selective surface erosion. Erosion scarp is formed because fine sand particles are easier to be eroded away

Fig. 18 Relationship between vertical erosion rate and lake volume: (**a**) balance-grained dams; (**b**) fine-grained dams
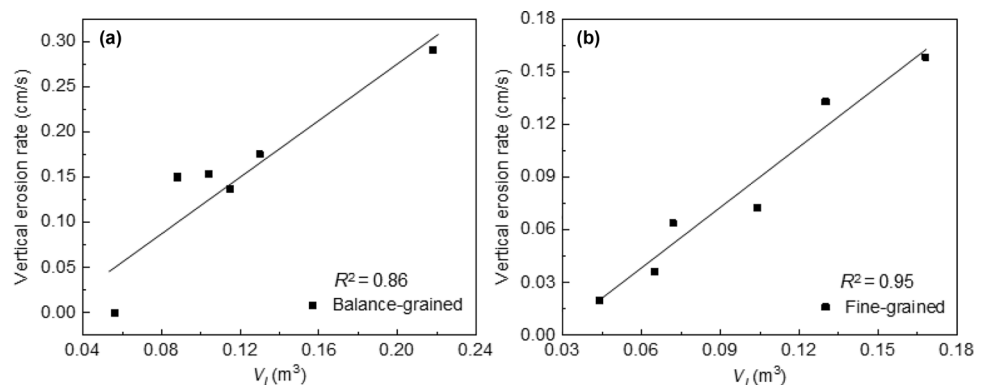
than coarse gravel particles (Fig. 9). However, the surface particles of fine-grained dams are uniformly eroded layer by layer, due to finer nature and narrow grading of the fine-grained debris (Fig. 10).

Effects of dam geometry on dam breaching

The morphology of the dam formed by natural accumulation is irregular, which is affected by material composition, sliding path width and valley shape (Fig. 4). Dam height and downstream slope have been studied by many scholars and shown to have considerable effects on the breaching process (Chinnarasri et al. 2003; Chen et al. 2015; Jiang and Wei 2020). All the dams in this study have different heights and downstream slopes because they are formed through a deposition process mimicking natural conditions. The results show that the arrival time of peak discharge is closely related to the dam height for balance-grained dams, while to the volume of the dammed lake for fine-grained dams (Fig. 14). However, the effect of downstream slope on the arrival time of peak discharge and peak discharge is not obvious (Fig. 19). The reason may be that the downstream slope of the tested dam formed through a deposition process is smaller than the angle of repose of the debris material, so the initial downstream slope has little effect on breach parameters. For the peak discharge, it depends on the volume of dammed lake and the volume released (Fig. 15). Nonetheless, it is challenging to predict the released water volume before the breach occurs. Therefore, the lake volume, which is affected by the dam height and the valley shape, is the key parameter in determining the peak discharge.

Unlike an artificially prebuild dam, which the elevation of cross-valley profile is always constant, landslide dams always have different shapes of cross-valley profiles (Mei et al. 2021; Zhou et al. 2021). The crest surface frontal angle, as a parameter to describe the cross-valley profile of the natural dam deposit, is most affected by the material (Fig. 4d). Regardless of valley shape and sliding width, the crest surface frontal angle increases as the mean grain diameter of the debris composition decreases. Furthermore, the crest surface frontal angle of fine-grained dams increases as the valley shape changes from rectangular to trapezoidal to triangular, approaching its angle of repose. This is the reason why the surface slide of dam crest (Fig. 10d) occurs in a fine-grained dam during the breaching process. Moreover, the surface sliding and lateral collapse result in secondary blockages and discharge fluctuations (Fig. 12e and f).

Effects of particle distribution on dam breaching

For the dams formed by the debris material with a wide size distribution (i.e., coarse-grained dam and balance-grained dam), the horizontal and vertical particle distributions of the dam are all different due to the particle segregation in the movement and accumulation process (Fig. 6). Overtopping starts normally at the lowest crest elevation (Fig. 3). Material properties on the location of the overflow point have a significant influence on the stability and failure mode of the dam. For example, coarse-grained dams were mostly stable except that overtopping erosion occurred in Test W-1C (Fig. 11b). This is due to the overflow point being located on the opposite side for most tests, where a higher concentration of coarse gravels resulted in a more stable structure. When the overflow point is located on the surface where most fine sands are concentrated, surface erosion will occur even if the dam height and the impoundment volume are small (e.g., Test W-1C). The critical initiation velocity v_c for cohesionless debris was estimated according to the formula proposed by Zhang et al. (2007) to assess the occurrence of erosion.

$$v_c = \left(\frac{h}{d} \right)^{0.14} \times \left(17.6 \frac{\gamma_s - \gamma}{\gamma} d \right)^{0.5} \tag{1}$$

where h is the flow depth (m), d is the particle diameter (m), and γ_s and γ are the bulk density of the deposit and flow, respectively. Based on the particle distribution on the surface of the dam deposit, the median diameter of the particles at the overflow location is considered the particle diameter d. The calculated v_c of the three debris compositions and the corresponding maximum flow velocity v during the breach process are shown in Table 4. When the overflow occurs on the opposite side, v_c was 0.58 m/s for coarse-grained debris, which is greater than the maximum flow velocity of 0.35 m/s in breaching process; hence, erosion was not initiated under surface flow. For Test W-1C, v_c was about 0.43 m/s because the overflow point is located on the source side with a higher concentration of sand, and the maximum flow velocity was about 0.56 m/s; therefore, erosion occurred on the surface of coarse-grained dam in this test.

In addition, due to the fact that the distribution of coarse particles inside the balance-grained dam was less than that on the surface (Fig. 6d and e), lateral erosion was more likely to develop with an increase in breach depth. When the breach developed to a

Fig. 19 Relationship between breach parameters and downstream slope: (**a**) arrival time of peak discharge; (**b**) peak discharge
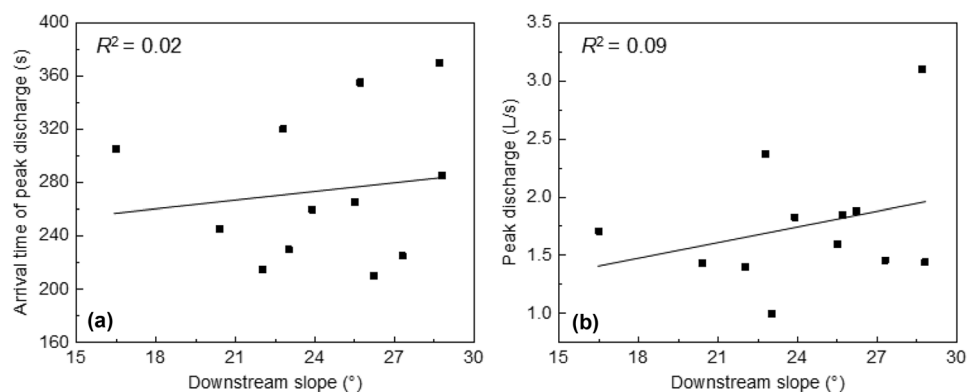
Table 4 Critical initiation velocity and the maximum flow velocity in tests

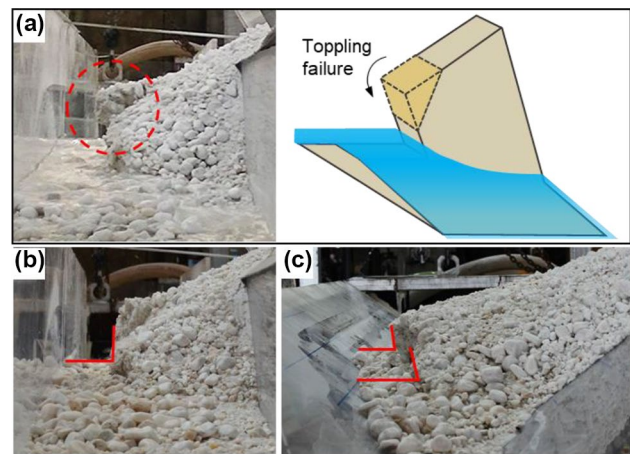| Material	Opposite side				Source side			
	d (mm)	v_c (m/s)	d (mm)	v (m/s)	d (mm)	v_c (m/s)	d (mm)	v (m/s)
Coarse-grained	18.9	0.58		0.35	7.2	0.43		0.56
Balance-grained	9.9	0.49		0.75	2.5	0.28		0.89
Fine-grained	0.86	0.16		0.94	-	-		-

Fig. 20 Breach side slope and final shape: (**a**) toppling failure of breach side slope; (**b**) Test N-1B; (**c**) Test N-3B

certain depth and width, the soil block of side slope toppled, which often occurred in a dam with cohesions (Fig. 20a). This phenomenon can be attributed to internal soil suction. With the increase of moisture content, the debris within the dam body became unsaturated and exhibited some cohesive behavior. The final shape of the breach was mostly rectangular or inverted trapezoid (Fig. 20b and c), which was consistent with the observation of dams completing consolidation (Zhong et al. 2019).

Conclusions

This study provides an improved understanding of the entire process from the formation of a landslide dam to its breaching via laboratory tests. The effects of valley shape, width of sliding path, and grain size distribution of the sliding mass on the dam characteristics and dam breaching are analyzed. The following conclusions specific to the test conditions have been reached as the result of this investigation:

1. The stability and failure modes of landslide dams are predominantly governed by the debris composition, whereas the valley shape and particle distribution also have an influence. The results of breaching can be classified into four categories: seepage equilibrium under overtopping, overtopping with scarp erosion, overtopping with layered erosion, and partial breaching without decrease in dam height.
2. Balance-grained dams have a longer duration for breach complete formation and a short duration for breach development, while the opposite is true for fine-grained dams. After breaching, an armoring layer will form at the bottom of the breach in balance-grained dams. Fine-grained dams are prone to secondary blockage during the river rebalancing phase, because of a high crest surface frontal angle.
3. The valley shape is a parameter that crucially affects the geometry of a landslide dam and the pre-dam storage capacity. Compared with dam height and downstream slope, peak discharge is more related to the released water volume and dammed lake volume. For balance-grained dams, the arrival time of peak flow is delayed with the increase in dam height, and the peak

discharge increases with the dammed lake volume. For fine-grained dams, the peak discharge and the arrival time are all positively correlated with the dammed lake volume.

4. Three new longitudinal evolution models are proposed to reveal the erosion characteristics of the breaching process, which are related to the debris composition and valley shape. The deposition of eroded material affects the development of downstream slope erosion. The first one is characterized by a constant downstream slope angle followed by a gradual decrease in the slope angle by rotating along a pivot point at the dam toe with continuing erosion. The second one is characterized by a concave shape along the longitudinal flow direction with the erosion point progressively moving to the dam crest. The last one is characterized by a progressive erosion with a decrease in erosion rate along the flow and downward direction.

Declarations

Conflict of interest   The authors declare no competing interests.

References

Casagli N, Ermini L, Rosati G (2003) Determining grain size distribution of the material composing landslide dams in the Northern Apennines: sampling and processing methods. Eng Geol 69(1–2):83–97

Chang DS, Zhang LM (2010) Simulation of the erosion process of landslide dams due to overtopping considering variations in soil erodibility along depth. Nat Hazards Earth Syst Sci 10(4):933–946

Chang DS, Zhang LM, Xu Y, Huang RQ (2011) Field testing of erodibility of two landslide dams triggered by the 12 May Wenchuan earthquake. Landslides 8:321–332

Chen SC, Lin TW, Chen CY (2015) Modeling of natural dam failure modes and downstream riverbed morphological changes with different dam materials in a flume test. Eng Geol 188:148–158

Chinnarasri C, Tingsanchali T, Weesakul S, Wongwises S (2003) Flow patterns and damage of dike overtopping. Int J Sedim Res 18(4):301–309

Costa JE (1985) Floods from dam failures. US Geol Surv Open-File Rep 85–560:54

Costa JE, Schuster RL (1988) The formation and failure of natural dams. Geol Soc Am Bull 100(7):1054–1068

Cui P, Zhu YY, Han YS, Chen XQ, Zhuang JQ (2009) The 12 May Wenchuan earthquake-induced landslide lakes: distribution and preliminary risk evaluation. Landslides 6(3):209–223

Dai LX, Fan XM, Jansen JD, Xu Q (2021) Landslides and fluvial response to landsliding induced by the 1933 Diexi earthquake, Minjiang River, eastern Tibetan Plateau. Landslides 18(9):3011–3025

Delaney KB, Evans SG (2015) The 2000 Yigong landslide (Tibetan Plateau), rockslide-dammed lake and outburst flood: review, remote sensing analysis, and process modelling. Geomorphology 246:377–393

Dunning SA, Armitage PJ (2011) The grain-size distribution of rock-avalanche deposits: implications for natural dam stability. Natural and artificial rockslide dams. Springer, Berlin, Heidelberg, pp 479–498

Fan XY, Qiao JP (2010) Influence of landslide and ground factors on large-scale landslide movement. Chin J Rock Mech Eng 29(11):2337 (In Chinese)

Fan XM, Scaringi G, Korup O et al (2019) Earthquake-induced chains of geologic hazards: patterns, mechanisms, and impacts. Rev Geophys 57(2):421–503

Fan XM, Dufresne A, Subramanian SS et al (2020) The formation and impact of landslide dams–state of the art. Earth Sci Rev 203:103116

Iverson RM, Logan M, LaHusen RG, Berti M (2010) The perfect debris flow? Aggregated results from 28 large-scale experiments. J Geophys Res Earth Surface 115(F3)

Iverson RM (2015) Scaling and design of landslide and debris-flow experiments. Geomorphology 244:9–20

Jiang XG, Huang JH, Wei YW, Niu ZP, Chen FH, Zou ZY, Zhu ZY (2018) The influence of materials on the breaching process of natural dams. Landslides 15(2):243–255

Jiang XG, Wei YW (2020) Erosion characteristics of outburst floods on channel beds under the conditions of different natural dam downstream slope angles. Landslides 17(8):1823–1834

Kuo YS, Tsang YC, Chen KT, Shieh CL (2011) Analysis of landslide dam geometries. J Mt Sci 8(4):544–550

Liu W, He SM (2018) Dynamic simulation of a mountain disaster chain: landslides, barrier lakes, and outburst floods. Nat Hazards 90(2):757–775

Mei SY, Chen SS, Zhong QM, Shan YB (2021) Effects of grain size distribution on landslide dam breaching—insights from recent cases in China. Front Earth Sci 9:245

Peng M, Zhang LM (2012) Breaching parameters of landslide dams. Landslides 9(1):13–31

Powledge GR, Ralston DC, Miller P, Chen YH, Clopper PE, Temple DM (1989) Mechanics of overflow erosion on embankments. II: Hydraulic and design considerations. J Hydra Eng 115(8): 1056–1075

Roessler T, Richter C, Katterfeld A, Will F (2019) Development of a standard calibration procedure for the DEM parameters of cohesionless bulk materials–part I: Solving the problem of ambiguous parameter combinations. Powder Technol 343:803–812

Ruan HC, Chen HY, Li Y, Chen JG, Li HB (2021) Study on the downcutting rate of a debris flow dam based on grain-size distribution. Geomorphology 391:107891

Schmocker L, Hager WH (2009) Modelling dike breaching due to overtopping. J Hydraul Res 47(5):585–597

Schilirò L, Esposito C, De Blasio FV, Scarascia Mugnozza G (2019) Sediment texture in rock avalanche deposits: insights from field and experimental observations. Landslides 16(9):1629–1643

Shang YJ, Yang ZF, Li LH, Liu DA, Liao QL, Wang YC (2003) A super-large landslide in Tibet in 2000: background, occurrence, disaster, and origin. Geomorphology 54(3–4):225–243

Shen DY, Shi ZM, Peng M, Zhang LM, Jiang MZ (2020) Longevity analysis of landslide dams. Landslides 17(8):1797–1821

Visser PJ (1998) Breach growth in sand-dikes. Dissertation, Delft University of Technology

Walder JS, O'Connor JE (1997) Methods for predicting peak discharge of floods caused by failure of natural and constructed earthen dams. Water Resour Res 33(10):2337–2348

Xu Q, Fan XM, Huang RQ, Westen CV (2009) Landslide dams triggered by the Wenchuan Earthquake, Sichuan Province, south west China. Bull Eng Geol Env 68(3):373–386

Yang Y, Cao SY, Yang KJ, Li WP (2015) Experimental study of breach process of landslide dams by overtopping and its initiation mechanisms. J Hydrodyn 27(6):872–883

Yin Y, Wang F, Sun P (2009) Landslide hazards triggered by the 2008 Wenchuan earthquake, Sichuan. China Landslides 6(2):139–152

Zhang JY, Fan G, Li HB, Zhou JW, Yang XG (2021) Large-scale field model tests of landslide dam breaching. Eng Geol 293:106322

Zhang RJ, Xie JH, Chen WB (2007) River dynamics. Wuhan University Press: Wuhan, China, pp 46–60 (In Chinese)

Zhao GW, Jiang YJ, Qiao JP, Yang ZJ, Ding PP (2019) Numerical and experimental study on the formation mode of a landslide dam and its influence on dam breaching. Bull Eng Geol Env 78(4):2519–2533

Zheng HC, Shi ZM, Shen DY, Peng M, Hanley KJ, Ma CY, Zhang LM (2021) Recent advances in stability and failure mechanisms of landslide dams. Front Earth Sci 9:201

Zheng HC, Shi ZM, Peng M, Guan SG, Hanley KJ, Feng SJ (2022) Amplification effect of cascading breach discharge of landslide dams. Landslides, 1–15

Zhong QM, Chen SS, Mei SA, Cao W (2018) Numerical simulation of landslide dam breaching due to overtopping. Landslides 15(6):1183–1192

Zhong QM, Chen SS, Deng Z, Mei SA (2019) Prediction of overtopping-induced breach process of cohesive dams. J Geotech Geoenviron Eng 145(5):04019012

Zhou GGD, Zhou MJ, Shrestha MS et al (2019a) Experimental investigation on the longitudinal evolution of landslide dam breaching and outburst floods. Geomorphology 334:29–43

Zhou YY, Shi ZM, Zhang QZ, Jang B, Wu CZ (2019b) Damming process and characteristics of landslide-debris avalanches. Soil Dyn Earthq Eng 121:252–261

Zhou YY, Shi ZM, Zhang QZ, Liu WR, Peng M, Wu CZ (2019c) 3D DEM investigation on the morphology and structure of landslide dams formed by dry granular flows. Eng Geol 258:105151

Zhou YY, Shi ZM, Qiu T, Yu SB, Zhang QZ, Shen DY (2021) Experimental study on morphological characteristics of landslide dams in different shaped valleys. Geomorphology 108081

Zhu XH, Peng JB, Liu BX, Jiang C, Guo J (2020) Influence of textural properties on the failure mode and process of landslide dams. Eng Geol 271:105613

Zhu XH, Liu BX, Peng JB et al (2021) Experimental study on the longitudinal evolution of the overtopping breaching of noncohesive landslide dams. Eng Geol 288:106137

Yuanyuan Zhou · Zhenming Shi · Hongchao Zheng (✉)
Department of Geotechnical Engineering, Tongji University,
Shanghai 200092, China
Email: 1410274@tongji.edu.cn

Yuanyuan Zhou · Zhenming Shi · Hongchao Zheng
Key Laboratory of Geotechnical and Underground Engineering
of Ministry of Education, Tongji University, Shanghai 200092, China
Email: 1410274@tongji.edu.cn

Tong Qiu
Department of Civil and Environmental Engineering, The
Pennsylvania State University, State College, University Park,
PA 16802, USA